arXiv:astro-ph/9808156v1 14 Aug 1998

Redshift determination in the X–ray band of gamma–ray bursts

Gabriele Ghisellini
Osservatorio Astronomico di Brera, Via Bianchi 46, I–23807 Merate, Italy

Francesco Haardt
Dipartimento di Fisica dell'Università di Como, via Lucini 3, I–22100 Como, Italy

Sergio Campana, Davide Lazzati[1], Stefano Covino
Osservatorio Astronomico di Brera, Via Bianchi 46, I–23807 Merate, Italy
[1] Dipartimento di Fisica dell'Università di Milano, Via Celoria 16, I–20133 Milano, Italy

ABSTRACT

If gamma–ray bursts originate in dense stellar forming regions, the interstellar material can imprint detectable absorption features on the observed X–ray spectrum. Such features can be detected by existing and planned X–ray satellites, as long as the X–ray afterglow is observed after a few minutes from the burst. If the column density of the interstellar material exceeds $\sim 10^{23}$ cm^{-2} there exists the possibility to detect the K_α fluorescent iron line, which should be visible for more than one year, long after the X–ray afterglow continuum has faded away. Detection of these X–ray features will make possible the determination of the redshift of gamma–ray bursts even when their optical afterglow is severely dimmed by extinction.

Subject headings: gamma rays: bursts — Line: formation — X rays: general — X rays: lines

1. Introduction

After the breakthrough of BeppoSAX in gamma–ray burst science (Costa et al. 1997; Van Paradijs et al. 1997), to solve the mystery of the origin of gamma–ray bursts we still need to build up a sizeable sample of objects with known redshift. Optical spectroscopy is however difficult, as both the optical afterglow and the presumed host galaxy are faint. Moreover, the optical afterglow is not observed in nearly half of the bursts with observed X–ray afterglows: a possible explanation is optical extinction, favoring models in which the bursts are formed in dense regions of stellar formation (Paczyński 1998).

If this is the case, the typical densities (of hydrogen atoms) is of the order of $n \sim 10^4$–10^5 cm^{-3}, with typical sizes of tens of parsecs. It is therefore conceivable to

have column densities $N_{\rm H}\gtrsim 10^{22}$ cm^{-2}, which would, besides heavily reddening the optical emission of the bursts, also absorb their X–ray spectra. GRB970828 observed by ASCA (Murakami 1998) and GRB980329 observed by BeppoSAX (in't Zand et al. 1998) have already given some evidence of intrinsic high column densities. The possibility exists, therefore, to observe absorption edges in the X–ray spectra of gamma–ray burst afterglows. This would lead to the determination of the redshift using only X–ray data, as long as the observations are carried out when the decaying X–ray afterglow is sufficiently bright. Along these lines, Loeb & Perna (1998) discussed the time behavior of optical absorption lines, and Mészáros & Rees (1998) discussed the possibility to observe broad absorption features originating in the relativistic fireball, and qualitatively investigated the detectability of iron emission lines in the X–ray spectra of bursts.

In this paper we investigate the detectability of X–ray features in detail, finding which part of the $N_{\rm H}$–redshift plane can be accessed by present and future X–ray missions.

If bursts (or a fraction of them) originate in dense regions, then also the re-emission of the absorbed energy should be important. In the X–ray band, the most prominent emission feature will probably be the fluorescent K_α iron line. We then calculate the expected flux of this line and its light curve, to see if and when it can be detected.

2. The $N_{\rm H}$–redshift plane

In Fig. 1 we show the X–ray spectra observed assuming different values of $N_{\rm H}$, located at $z = 0$, and an intrinsic power law photon spectrum $\propto \epsilon^{-1}$, where ϵ is the photon energy. The cut–off frequency produced by absorption gives a relation between $N_{\rm H}$ and z, since a small cut–off frequency can be produced by a small column at a small redshift, or a large column at a large redshift. To disentangle this degeneracy we must detect some absorption edges.

The absorption edges are more prominent for larger $N_{\rm H}$, but the observed flux is dimmer. The detectability of a particular edge will therefore be possible only in a range of $N_{\rm H}$, depending on the particular considered edge, the intrinsic (unabsorbed) flux of the burst, the integration time and the effective area of the detector.

Let C_1' and C_2' be the number of counts in the energy bins just below and just above an absorption edge. If C_1' and C_2' are independent measures of the number of success in two stochastic processes, we can say that C_1' differs from C_2' at a level of f sigma if:

$$C_1' - C_2' > f\sqrt{C_1' + C_2'} \tag{1}$$

The observed counts are related to the 'unabsorbed' counts (that we would have observed with $N_{\rm H} = 0$) by $C_1' = C_1 e^{-\tau_1}$ and $C_2' = C_2 e^{-\tau_2}$, where τ_1 and τ_2 are the absorption

optical depths at energies just below and above the edge.

In addition, since the two energy bins are centered at the two energies ϵ_1 and ϵ_2, we have $C_2 = C_1(\epsilon_2/\epsilon_1)^{-\Gamma}$, where Γ is the photon spectral index. Then we have

$$C_1 > f^2 \frac{e^{-\tau_1} + (\epsilon_1/\epsilon_2)^{\Gamma} e^{-\tau_2}}{\left[e^{-\tau_1} - (\epsilon_1/\epsilon_2)^{\Gamma} e^{-\tau_2}\right]^2} \tag{2}$$

The optical depth below and above the edge can be approximated by a polynomial function (e.g. Balucinska–Church & McCammon 1992). As an example, the optical depths below and above the neutral oxygen (at 0.521 keV) and neutral iron (at 7.111 keV) edges, for solar abundances, are $\tau_{1,O} \simeq 652.3\,\tau_T$; $\tau_{2,O} \simeq 1095.2\,\tau_T$; $\tau_{1,Fe} \simeq 1.265\,\tau_T$; $\tau_{2,Fe} \simeq 2.360\,\tau_T$, where τ_T is the Thomson scattering optical depth.

In Fig. 2 we show the minimum number of counts (i.e. C_1) necessary to detect the neutral oxygen and the neutral iron edges, as a function of $N_{\rm H}$, calculated as above. The solid lines in Fig. 2 correspond to Equation (2) (for f =1, 2, 3), while dashed lines correspond to the actual number of counts detected, taking into account absorption (i.e. they correspond to $C' = Ce^{-\tau_1}$). It can be noted that this simple estimate refers only to the number of counts in two bins (immediately below and immediately above) the edge energy. However, we should add also the information contained into the other adjacent bins, increasing the detectability of the edge. We can therefore consider Equation (2) and Fig. 2 as a conservative, albeit rough, estimate.

Fig. 2 shows the range of $N_{\rm H}$ at which a particular detector is sensitive. For a given effective area, exposure time and *unabsorbed* flux, we can estimate the number of counts that would be detected (in the absence of absorption). This can be represented by an horizontal line on Fig. 2, intercepting the solid lines in two points, which defines the extremes of the range of $N_{\rm H}$ for which we can see the considered edge. The actual observed counts (including absorption) are then given by the dashed lines.

Analogously, Fig. 2 can be used to estimate the exposure time needed to detect the edge once we know the observed (absorbed) flux (dashed lines). This is given by the dashed lines in Fig. 2, by dividing the known flux by the required counts and by the effective area. In this case, the solid lines give the corresponding unabsorbed flux.

3. Simulations

Let A be the effective area of the X–ray detector, and F the integrated flux of the burst in a given energy band, between ϵ_1 and ϵ_2. In general, A will be a function of frequency, while F a function of time. Although we still lack information on the detailed behavior of the X–ray flux soon after the burst, let assume a power law behavior, connecting the flux at the time of burst and the afterglow as seen a few hours later. We know that $\sim$ 10 hours

after the burst, the observed 2–10 keV flux is of the order of $\sim 10^{-13}$ erg cm^{-2} s^{-1} (in't Zand et al. 1998; Frontera et al. 1998; Piro et al. 1998a, 1998b). Assuming a t^{-1} dependence, we obtain a flux of $F(t = 100 \text{ s}) = 3.6 \times 10^{-9}$ erg cm^{-2} s^{-1} during, or immediately after, the burst [corresponding to a monochromatic flux of 160 μJy if the energy spectral index is flat ($\Gamma = 1$)].

For $\Gamma = 1$ the counts detected in t_{exp} exposure time, starting at t_1, in the energy bin $\Delta\epsilon$ are

$$\begin{aligned} C' &= A\,F(t_1)\,\frac{\Delta\epsilon}{\epsilon}\,\frac{1}{\epsilon_2-\epsilon_1}\ln(t_{exp}/t_1) \\ &\approx 62.4\left(\frac{A}{100\text{ cm}^2}\right)\left(\frac{F(t_1)}{10^{-8}\text{ erg cm}^{-2}\text{ s}^{-1}}\right)\left(\frac{\Delta\epsilon/\epsilon}{0.1}\right)\frac{\ln(t_{exp}/t_1)}{\epsilon_{2,\text{keV}}-\epsilon_{1,\text{keV}}} \end{aligned} \quad (3)$$

Given the assumed time decay law and energy spectrum, the necessary S/N ratio can be achieved only if the X–ray observation starts immediately after the burst itself, or if the collecting effective area of the detector is much larger than 100 cm^2.

We have simulated the observed spectrum by using the response matrices of some future planned missions, such as JET-X ($A \sim 200$ cm^2 at 1.5 keV and $A \sim 40$ cm^2 at 8.1 keV for the two telescopes; Citterio et al. 1996), AXAF with Back Illuminated (BI) CCDs ($A \sim 700$ cm^2 at 1.5 keV and $A \sim 40$ cm^2 at 8.1 keV; Kellogg et al. 1997) and XMM with the EPIC detectors ($A \sim 3600$ cm^2 at 1.5 keV and $A \sim 1500$ cm^2 at 8.1 keV for three telescopes; Gondoin et al. 1996) and assuming: i) $F(t_1) = 10^{-8}$ between 2 and 10 keV at the beginning of the observation; ii) a power law time decay of the flux $\propto t^{-1}$; iii) an intrinsic (unabsorbed) power law spectrum of photon index $\Gamma = 1$ in the considered energy range, constant in time. We considered these three telescopes because they cover a wide range of effective areas, have a good spectral resolution and allow for a low background contamination.

We simulated two different cases: a GRB afterglow at $z = 0.25$ and intrinsic $N_{\rm H} = 3 \times 10^{21}$ cm^{-2} and $z = 4$ and $N_{\rm H} = 10^{24}$ cm^{-2}, which are relevant for the oxygen and iron edge, respectively. A galactic column density of 3×10^{20} cm^{-2} has also been included.

In the case of the oxygen edge (at 0.52 keV) the satellite energy band is extremely important in order to recover the correct GRB redshift. In the case of JET-X, the minimum energy of 0.3 keV limits the maximum detectable redshift to ~ 0.7. The influence of the galactic absorption plays also a crucial role, such that only for low values ($\lesssim 5 \times 10^{20}$ cm^{-2}) we are able to disentangle the intrinsic and galactic absorption. In Fig. 3 we report the contour plots in the $N_{\rm H} - z$ plane of the simulated models as observed with different X–ray satellites. The three contours refer to 1, 2 and 3 σ confidence levels. In Fig. 3a is shown the case of the JET-X telescope. It can be noted that the input redshift and column density are not recovered satisfactorily. In particular, the presence of different absorption features (O, Ne, Mg, Si) results in the elongated contour in the $N_{\rm H} - z$ plane. In the case of AXAF (Fig.

3b), the recovery of the GRB redshift is eased by the higher throughput at low energies guaranteed by the BI CCDs. The large effective area of XMM poses no problem for the identification of the redshift (Fig. 3c).

In the case of the Fe edge there are less problems due to the fact that beyond iron there are not prominent K edges. This is testified by Fig. 4, in which for all the considered instrument the redshift and the column density are recovered with a high degree of confidence.

4. Re-emission of the fluorescent K_α iron line

The dense material responsible for the absorption we have discussed in the previous sections will re-emit the absorbed energy, and part of it will be re-emitted in the form of X–ray lines. Among those, the fluorescent K_α iron line will be the most prominent. A very crude estimate of the expected flux can be done by assuming that a fraction a of the fluence $\mathcal{F}$ emitted by the burst is re-emitted by a region of dimension R, in an observed time-scale of the order of R/c. Then the average flux of the iron fluorescent K_α line is

$$F_{K_\alpha} \approx \frac{a\,\mathcal{F}}{R/c} \approx 10^{-16} \left(\frac{a}{0.01}\right) \left(\frac{\mathcal{F}}{10^{-5}\,\mathrm{erg\ cm^{-2}}}\right) \left(\frac{1\ \mathrm{pc}}{R}\right)\ \mathrm{erg\ cm^{-2}\ s^{-1}} \tag{4}$$

This promising result motivates a somewhat deeper analysis.

At the energy of the neutral iron edge and assuming a solar abundance of iron, the optical depth for photoelectric absorption is $\tau_{7.1} \sim 2.36\,\tau_T$ and increases somewhat for partially ionized iron. The incoming ionizing flux preferentially photoionizes an electron of the iron K shell, instead of electrons of outer shells, because lower energy photons are preferentially absorbed by lighter elements. The absorption is immediately followed by fluorescence emission of a K_α photon whose energy ranges between 6.4 and 6.9 keV, depending on the ionization state. An initially neutral iron atom can therefore absorb up to a maximum of 26 ionizing photons. Setting n the number density of hydrogen, the absorption optical depth for solar abundance, as long as the iron atoms are not completely ionized, is

$$\tau_{edge} \approx 0.5 \left(\frac{n}{10^5\ \mathrm{cm^{-3}}}\right) \left(\frac{R}{1\ \mathrm{pc}}\right) \tag{5}$$

If the bursts are located in a dense star forming region it is very likely that a significant fraction of the energy above the iron edge is absorbed.

Assuming that a fraction τ_{edge} (with $\tau_{edge} \leq 1$) of all photons between ϵ_{edge} and $2\,\epsilon_{edge}$ get absorbed, the energy re-emitted in the K_α line is a fraction $Y\tau_{edge}\epsilon_{edge}/\epsilon_{max}$ of the

total energy of the burst, where Y is the yield (equal to 0.37 for neutral iron, and larger for partially ionized iron), ϵ_{edge} is the edge energy, and ϵ_{max} is the energy where the burst spectrum peaks [in a $\epsilon F(\epsilon)$ representation]. The average flux received in the iron line is

$$\begin{aligned} F_{K_\alpha} &\simeq Y \tau_{edge} \frac{\epsilon_{edge}}{\epsilon_{max}} \frac{\mathcal{F}}{R/c} \\ &\approx 5.8 \times 10^{-16} \left(\frac{Y}{0.5}\right) \left(\frac{n}{10^5\,\mathrm{cm}^2}\right) \left(\frac{\mathcal{F}}{10^{-5}\,\mathrm{erg\ cm}^{-2}}\right) \left(\frac{\epsilon_{edge}/\epsilon_{max}}{0.025}\right) \quad \mathrm{erg\ cm}^{-2}\ \mathrm{s}^{-1} \end{aligned} \tag{6}$$

The line flux does not explicitly depend upon the dimension R, which however controls the duration of the line emission ($\sim R/c$). This dimension can be estimated by equating the number of ionizing photons to the total number of iron atoms present in a sphere of radius R, assuming that each iron atom absorbs 26 ionizing photons and a solar abundance x_{Fe} of iron:

$$N_{edge} \simeq \frac{E}{\epsilon_{max}} \frac{\Delta\epsilon}{\epsilon_{edge}} \simeq 26\, x_{Fe}\, n \frac{4\pi R^3}{3} \tag{7}$$

$$R \approx 0.65 \left[\left(\frac{E_{52}}{\epsilon_{300}}\right) \left(\frac{\Delta\epsilon}{\epsilon_{edge}}\right) \left(\frac{3\times 10^{-4}}{x_{Fe}}\right) \left(\frac{10^5\,\mathrm{cm}^{-3}}{n}\right) \right]^{1/3} \quad \mathrm{pc} \tag{8}$$

where $E = 10^{52}\, E_{52}$ erg is the total burst energy, whose spectrum peaks at $\epsilon_{max} = 300\,\epsilon_{300}$ keV. Note that with $n = 10^5\,\mathrm{cm}^{-3}$ and R given by Equation (12) one obtains a column of $N_{\rm H} \sim 2 \times 10^{23}$ cm^{-2}. The K_α iron line calculated in this simplified way is approximately constant for 2 years (but see below), long after the X–ray afterglow has decayed below the detection threshold (the 2–10 keV X–ray flux should be 10^{-16} erg cm^{-2} s^{-1} after a month, assuming a flux of 10^{-13} erg cm^{-2} s $^{-1}$ after ~ 10 hours). The line flux should be narrowly concentrated in the observed energy range $[6.9 - 6.4]/(1+z)$ keV. In the following section we present a detailed calculation for the light curve behavior of the line flux, including self consistently the effect of the absorption of the ionizing flux.

4.1. The light curve of the iron fluorescence line

Emission of fluorescence line photons can be treated as a scattering process, with each iron atom scattering off 26 ionizing photons. In order to compute the light curve of the scattered radiation in a spherical geometry, assuming that the ionizing photons come from a point–like central source, one has to consider the effects of the time–delays induced by geometry. A comprehensive treatment of a similar problem has been done by Blandford & McKee (1992), in the context of reverberation of the broad line region of AGNs, responding to a variable photoionizing central source. They however neglected the absorption term

of the ionizing flux, which instead is important here. Assuming, for semplicity, an infinite medium, it is not difficult to show that the flux of scattered photons is given by

$$\dot{N}_{\rm line}(t) \, = 2\pi Y \int_{-1}^{+1} d\mu \, \int_{R_{\rm min}}^{R_{\rm max}} dr \, r^2 n_F(r) \int_{\nu_0}^{\infty} \frac{d\nu}{h\nu} \, \frac{L_\nu(t')}{4\pi r^2} \, \sigma_\nu \, {\rm e}^{-\int_0^r dr' n_F(r') \sigma_\nu} \tag{9}$$

where r is the radial distance of the scattering event from the central source and μ is the cosine of the scattering angle. The values of r and μ are related to the arrival time t through $t = t' + (1-\mu)\, r/c$, where t' is the time of photons arriving directly, without being scattered. L_ν is the source specific luminosity. The factor Y is the fluorescence yield, n_F is the scattering material number density, i.e., in our case, it is 26 times the iron number density and σ_ν is the photoelectric cross section. The minimum and maximum value of the integration radius are given by the conditions $t' \geq 0$ and $t' \leq \Delta t$, where we assumed the source light curve to be steady for a duration Δt. Under such assumption we have $R_{\rm min} = \max[0, c\,(t - \Delta t)/(1-\mu)]$ and $R_{\rm max} = c\, t/(1-\mu)$.

The above integral can be worked out if one neglects the frequency dependence of the cross section and of the ionizing flux, and assuming further an homogeneous scattering medium. In this case

$$\int_{\nu_0}^{\infty} d\nu \frac{L_\nu(t')}{h\nu} \, \sigma_\nu \, {\rm e}^{-\int_0^r dr' n_F(r') \sigma_\nu} \, = \, \frac{\dot{N}_{\rm ion}}{h} \frac{{\rm e}^{-r/r_F}}{r_F n_F} \tag{10}$$

where the scale radius $r_F = 1/(n_F \sigma_0)$ is the radius of unit optical depth and $\dot{N}_{\rm ion}$ is the ionizing photon flux. Equation (9) then simplifies in

$$\dot{N}_{\rm line}(t) = \frac{Y}{2} \dot{N}_{\rm ion} \int_{-1}^{+1} d\mu \, \int_{R_{\rm min}}^{R_{\rm max}} \frac{dr}{r_F} \, {\rm e}^{-r/r_F} \tag{11}$$

Finally, the solution of the above double integral can be expressed in terms of exponential integral function of second order, $E_2(x)$, as

$$\dot{N}_{\rm line}(t) \, = \, Y \, \dot{N}_{\rm ion} [1 - E_2(t/2t_F)] \tag{12}$$

for $t \leq \Delta t$, and

$$\dot{N}_{\rm line}(t) \, = \, Y \, \dot{N}_{\rm ion} [E_2((t-\Delta t)/2t_F) - E_2(t/2t_F)] \tag{13}$$

for $t \geq \Delta t$. The time t_F is defined as $t_F = r_F/c$. Note that $\int_0^\infty dt \dot{N}_{\rm line} = \Delta t \dot{N}_{\rm ion}$.

The resulting light curve shows a power law growth for a time $t \leq \Delta t$, when the line flux reaches its maximum, then slowly decays for a time scale of order t_F. After that time, the line flux decays exponentially. Very roughly, one can imagine the light curve of the line to be steady at level $Y \dot{N}_{\rm ion} \Delta t / t_F$ for a time t_F, then going rapidly to zero. If the ionized sphere were density bounded (i.e., the optical depth τ_0 of the scattering cloud is < 1), rather than radiation bounded as assumed so far, the fluorescence line flux would be at the same level as seen above, but the duration of the line emission would be shortened by a factor τ_0. In Fig. 5 we show some illustrative examples of the iron line light curve. Note the slow power law decay of the line flux ($\propto t^{-1/10}$).

4.2. Detectability of the iron fluorescence line

The detection with instruments such as BeppoSAX, ASCA, AXAF or JET-X crucially depends on the X–ray background collected within the detection cell. The BeppoSAX and ASCA Point Spread Function (PSF) is too large (with an Half Energy Width, HEW, of the order of a few arcmin) and results in a strong background which overwhelms the emission line. The good PSF of JET-X (HEW $\sim 25''$) makes this instrument able to detect the line and determine its redshift in $\sim 100 - 200$ ks (for an assumed line flux of a few$\times 10^{-16}$ erg cm^{-2} s^{-1}), even if at a low significance level. The limiting factor is the effective area at the line energy. For high redshift GRB afterglows, AXAF BI CCDs provide a larger effective area (see above), so that the line can be easily detected in about 100 ks (assuming the same flux). In the case of XMM a firm detection is obtained in the same amount of time and a determination of the line width is possible.

5. Discussion

We have shown in a simplified but analytical way that if gamma–ray bursts originate in a dense environment their X–ray spectra are modified by absorption, and the imprinted edges can be used to determine their redshifts.

Available information on the amount the absorption column in X–rays are scarce, due to the fact that large field of view instruments detecting the gamma–ray bursts (such as the WFC on BeppoSAX or BATSE on CGRO) have limited energy resolution and/or they are insensitive to soft X–ray photons, while the narrow field instruments can follow the X–ray afterglow only some hours after the gamma–ray event, when the X–ray flux has presumably faded away. Despite these difficulties, for the very bright burst GRB980329 it was possible to analyze the spectrum of the X–ray afterglow and the best fit requires a column $N_{\rm H} = (1.0 \pm 0.4) \times 10^{22}$ cm^{-2} (with $z = 0$, in't Zand et al 1998), much larger than the galactic value ($N_{\rm H}^{gal} \sim 9 \times 10^{20}$ cm^{-2}). Note that if the absorption is located at the redshift of GRB980329, then the column is $(1 + z)^3$ times larger (Paczyński 1998).

Other indirect evidence of X–ray absorption comes from the extinction estimated in the optical, from the fact that not all the bursts with a detected X–ray afterglow could be detected in the optical, and to explain very hard X–ray to gamma–ray spectra of the burst themselves.

Due to the fact that the oxygen and iron edges are the most prominent, there are two almost distinct accessible part of the redshift–column density plane, one characterized by a moderate $N_{\rm H} \sim 10^{21}$–10^{22} cm^{-2} and $z \sim 0.1$–0.5 (assuming a detector energy window cutting-off at 0.1 keV), and the other one characterized by a column larger than 10^{23}. Note that for a standard dust to gas ratio, a column of $N_{\rm H} = 10^{22}$ cm^{-2} corresponds to an optical extinction $A_V \sim 6$ mag, precluding the possibility to detect the optical afterglow. If, furthermore, it were not possible to perform spectroscopic optical observation of the

host galaxy (either because a precise position is lacking, or because it is too faint), then the X–rays could be the only mean to determine the redshift, especially for strong bursts located at $z > 2$–3, for which the iron edge lies in the most sensitive energy range of X–ray detectors.

For a detailed spectral analysis to be at all possible, we need large count statistics, implying that the X–ray afterglow (assuming its temporal decay follows the observed law also soon after the burst event) must be followed as soon as possible (i.e. within minutes).

A different case is instead possible if a sizeable fraction of the burst high energy emission is re-emitted in the form of the fluorescent K_α iron line at an intrinsic energy between 6.4 and 6.9 keV. In this case, possible if the absorbing material has $N_{\rm H} > 10^{23}$ cm^{-2}, one can detect the fluorescence iron line up to $\sim 1 - 2$ years after the burst event. The key factors are the telescope effective area, to increase the throughput, as well as the HEW, to limit the background. The predicted flux for strong bursts is at the level of a few 10^{-16} erg cm^{-2} s^{-1}, concentrated in the energy range $[6.9\text{–}6.4]/(1 + z)$, which is detectable with the planned missions such as Spectrum X–Gamma, AXAF, XMM and of course Constellation–X.

The case of GRB980425 (Soffitta et al. 1998), possibly associated with the supernova 1998bw (Wang & Wheeler 1998), deserves a specific discussion, due to its proximity. We cannot exclude the possibility that the gamma–ray burst emission is, in general, anisotropic, and that GRB980425 is a rare (because fainter) event of a burst seen misaligned (Ghisellini et al. 1998). Causes of anisotropy could be different amount of baryon loading at different angles, together with (but not necessarily) different energy deposition as a function of angle (e.g. Rees 1998). GRB980425 may then correspond to a burst seen with high baryon loading, small bulk Lorentz factor, lower total energy. In this case the Doppler time contraction is much less extreme than in normal bursts, resulting in a slow evolution of the afterglow light curves, while the duration of the gamma–ray event, being controlled by the primary engine, is unchanged. This may explain the normal duration of the γ–ray emission, the fact the optical flux reached its maximum long after the burst event, with a rising light curve, and the overall observed energetics. This idea necessarily implies a much larger energy (of the order of 10^{51} erg, or larger) being emitted at a different angle. If the environment of GRB980425 is dense enough, then it is possible to detect a very strong fluorescence iron line, with a flux of the order of 10^{-13} erg cm^{-2} s^{-1}, easily detectable by already flying satellites. Due to the importance of this detection, we plan to propose X–ray observation in the direction of the supernova 1998bw, even if there are not clear signs of absorption in the optical spectrum.

REFERENCES

Balucinska-Church M. & Mc Cammon D., 1992, ApJ, 400, 699

Blandford R.D. & McKee C.F., 1992, ApJ, 255, 219

Citterio O. et al. 1996, SPIE,,2805, 56

Costa E. et al. 1997, Nature, 387, 783

Frontera F. et al. 1998, ApJ, 493, L67

Ghisellini G. et al., 1998, in preparation

Gondoin P. et al., 1996, SPIE, 2808, 390

in't Zand J.J.M. et al., 1998, ApJ (Lett) in press astro-ph/9807314

Kellogg E.M. et al., 1997, SPIE, 3113, 515

Loeb A. & Perna R., 1998, ApJ, 501, 467

Mészáros P. & Rees M.J., 1998, MNRAS in press (astro–ph/9806183, v2)

Murakami T., 1998, in proc. Fourth Huntsville Symp. on Gamma–Ray bursts, ed. C.A. Meegan, R. Preece & T.M. Koshut, in press

Paczyński B., 1998, ApJ, 494, L45

Piro L. et al., 1998a, A&A, 329, 906

Piro L. et al., 1998b, A&A, 331, L41

Rees M.J., 1998, in proc. of "The Active X-ray Sky: Results from BeppoSAX and Rossi-XTE", eds. L. Scarsi, H. Bradt, P. Giommi and F. Fiore, Nuclear Physics B Proceedings Supplements, in press

Soffitta P. et al., 1998, IAUC. 6884

van Paradijs J. et al., 1997, Nature, 386, 686

Wang L. & Wheeler J.C., 1998, ApJL in press

Wijers R.A.M.J., Rees M.J. & Mèszàros P., 1997, MNRAS, 288, L51

This preprint was prepared with the AAS LaTeX macros v4.0.

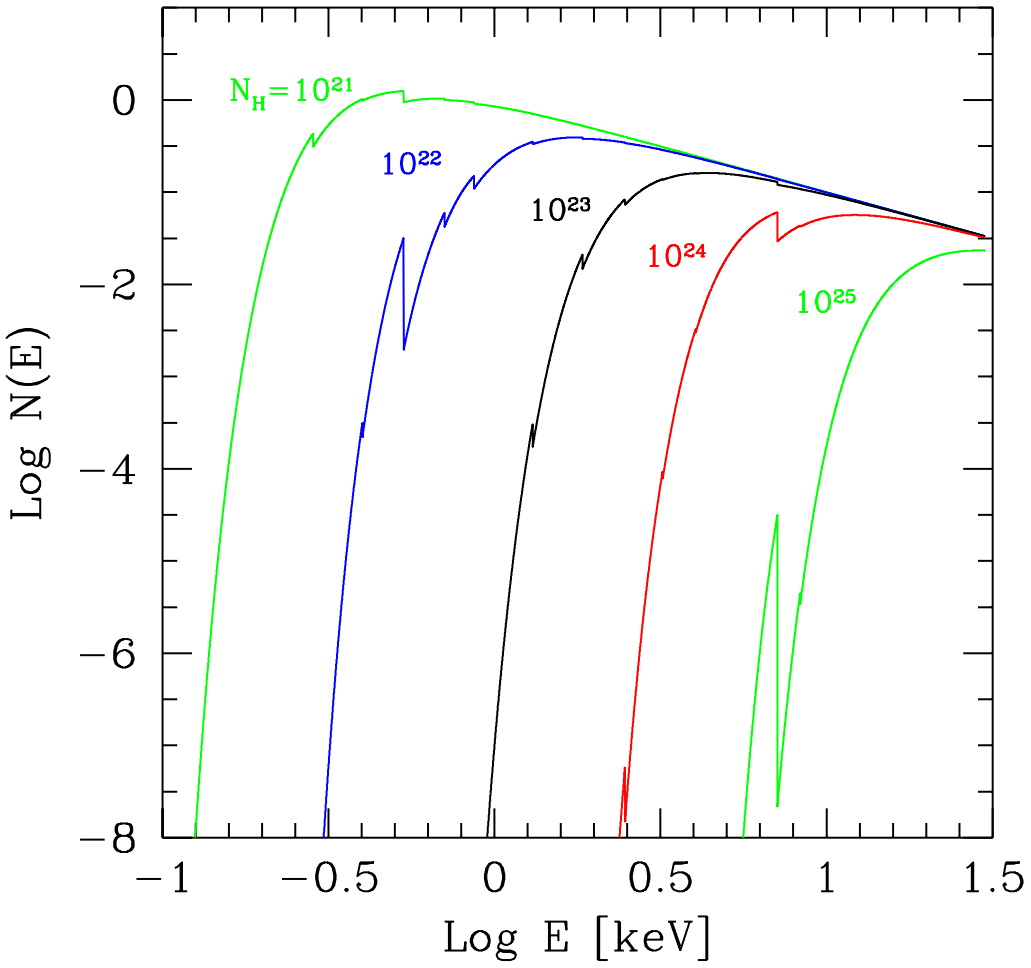

Fig. 1.— The effect of different amount of absorption on a power law spectrum with photon index $\Gamma = 1$. Labels indicate the values of $N_{\rm H}$ used. For this figure, we have assumed solar abundances of metals and that the absorption takes place at $z = 0$.

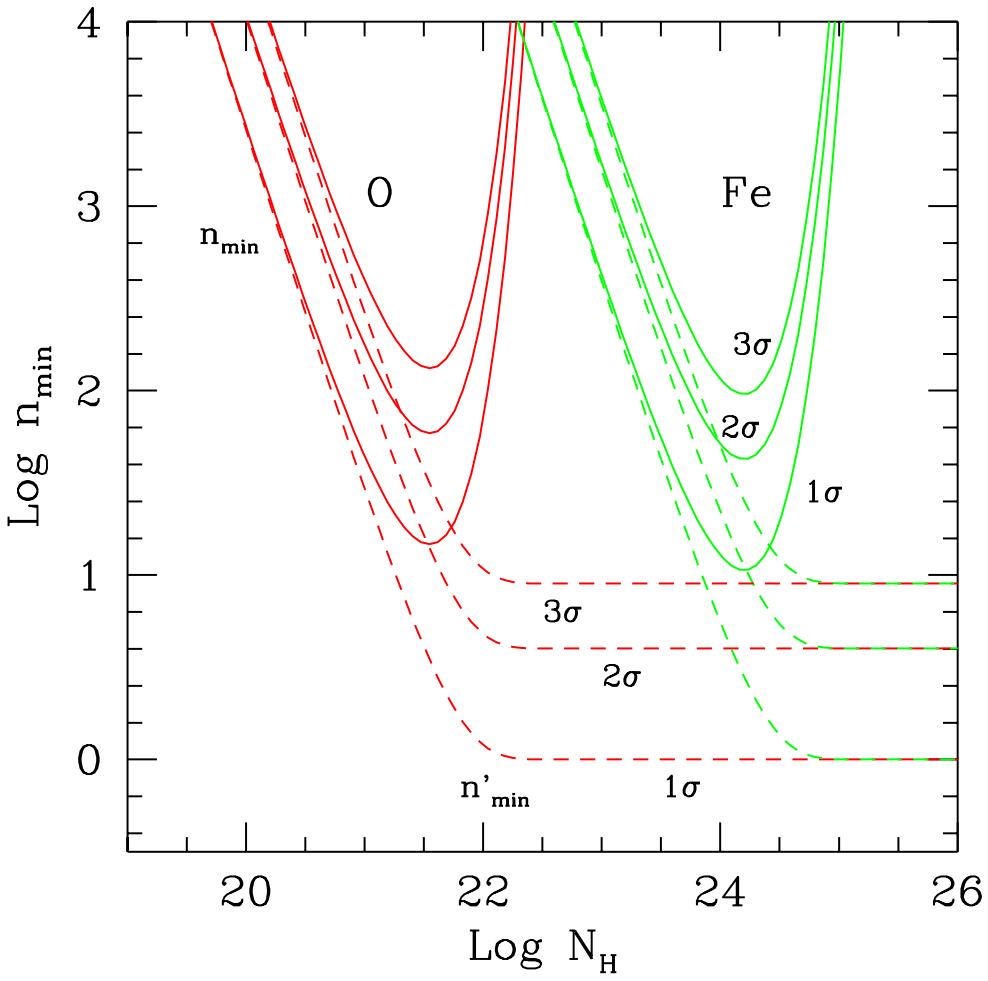

Fig. 2.— The counts required to detect (at 1, 2 and 3 sigma) the edge of neutral oxygen and neutral iron, as a function of the column density $N_{\rm H}$. The solid lines refer to the unabsorbed counts, while the dashed lines refer to the counts actually measured. Solar abundances of metals have been assumed.

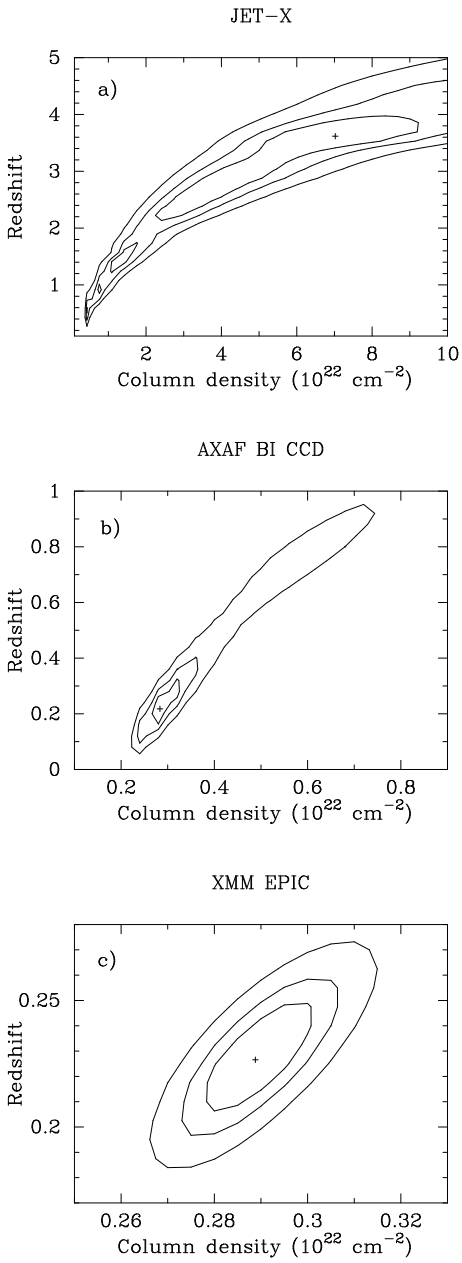

Fig. 3.— Column density – redshift contour plots for different X–ray instruments. The input model has $z = 0.25$ and $N_{\rm H} = 3 \times 10^{21}$ cm^{-2}. The upper panel (a) shows the case of JET-X (two telescopes). The middle panel (b) presents the case of AXAF with BI CCDs and the lower panel (c) the case of XMM (three telescopes). See text for more detail on the input parameters of the simulations.

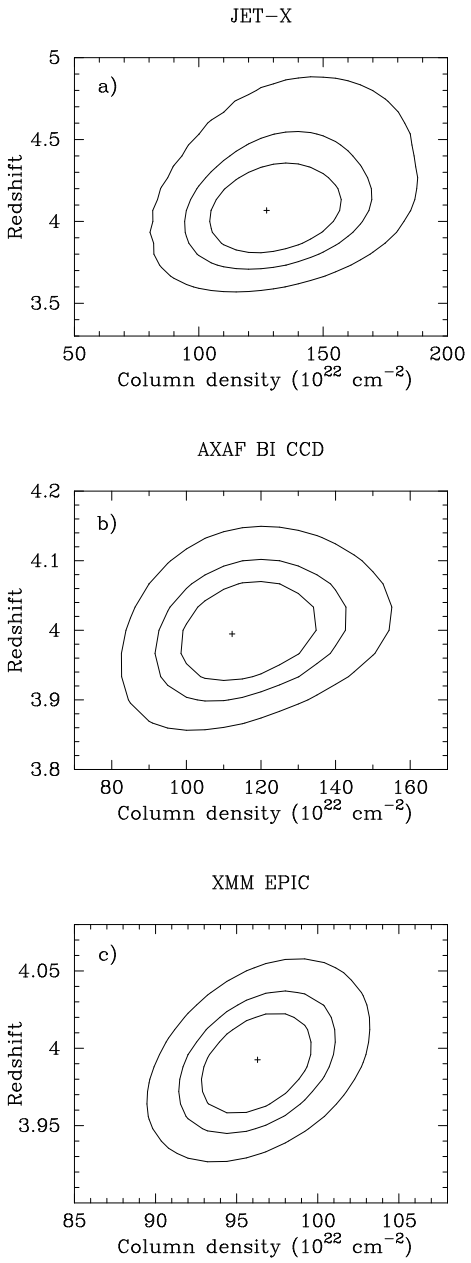

Fig. 4.— Column density – redshift contour plots for different X–ray instruments. The input model has $z = 4$ and $N_{\rm H} = 10^{24}$ cm^{-2}. The upper panel (a) shows the case of JET-X (two telescopes). The middle panel (b) presents the case of AXAF with BI CCDs and the lower panel (c) the case of XMM (three telescopes). See text for more detail on the input parameters of the simulations.

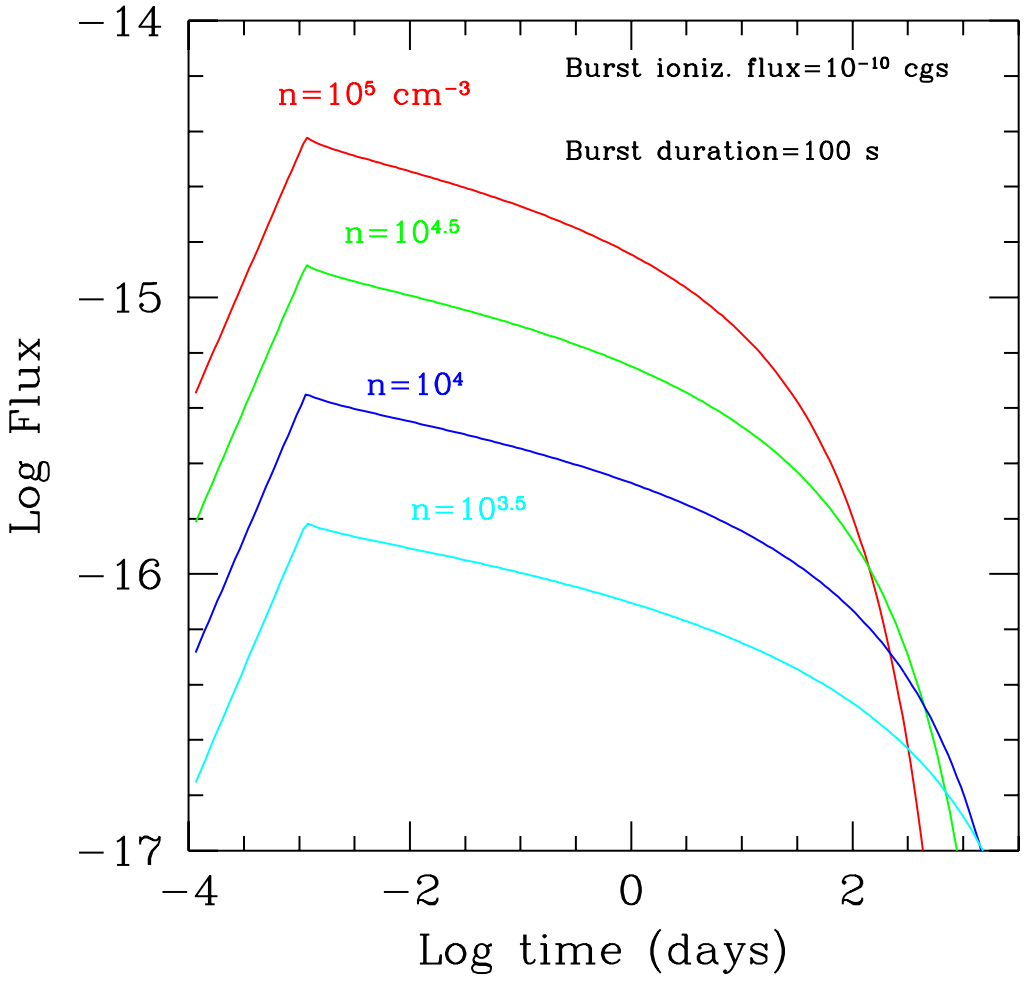

Fig. 5.— The iron fluorescence line light curve predicted for different values of the number density of hydrogen, assuming a solar abundance of iron and a burst of an ionizing flux of 10^{-10} erg cm^{-2} s^{-1} lasting for 100 seconds.